ACS Partner Journal

ENVIRONMENT & HEALTH

pubs.acs.org/EnvHealth

Article

Cellular Lipidome Changes during Retinoic Acid (RA)-Induced Differentiation in SH-SY5Y Cells: A Comprehensive *In Vitro* Model for Assessing Neurotoxicity of Contaminants

Michelle Camdzic, Diana S. Aga, and G. Ekin Atilla-Gokcumen*

Cite This: *Environ. Health* 2023, 1, 110–120

Read Online

ACCESS | Metrics & More | Article Recommendations | Supporting Information

ABSTRACT: The SH-SY5Y, neuroblastoma cell line, is a common *in vitro* model used to study physiological neuronal function and the neuronal response to different stimuli, including exposure to toxic chemicals. These cells can be differentiated to neuron-like cells by administration of various reagents, including retinoic acid or phorbol-12-myristate-13-acetate. Despite their common use, there is an incomplete understanding of the molecular changes that occur during differentiation. Therefore, there is a critical need to fully understand the molecular changes that occur during differentiation to properly study neurotoxicity in response to various environmental exposures. Previous studies have investigated the proteome and transcriptome during differentiation; however, the regulation of the cellular lipidome in this process is unexplored. In this work, we conducted liquid chromatography−mass spectrometry (LC−MS)-based untargeted lipidomics in undifferentiated and differentiated SH-SY5Y cells, induced by retinoic acid. We show that there are global differences between the cellular lipidomes of undifferentiated and differentiated cells. Out of thousands of features detected in positive and negative electrospray ionization modes, 44 species were identified that showed significant differences (p-value $\leq$0.05, fold change $\geq$2) in differentiated cells. Identification of these features combined with targeted lipidomics highlighted the accumulation of phospholipids, sterols, and sphingolipids during differentiation while triacylglycerols were depleted. These results provide important insights into lipid-related changes that occur during cellular differentiation of SH-5YSY cells and emphasize the need for the detailed characterization of biochemical differences that occur during differentiation while using this *in vitro* model for assessing ecological impacts of environmental pollutants.

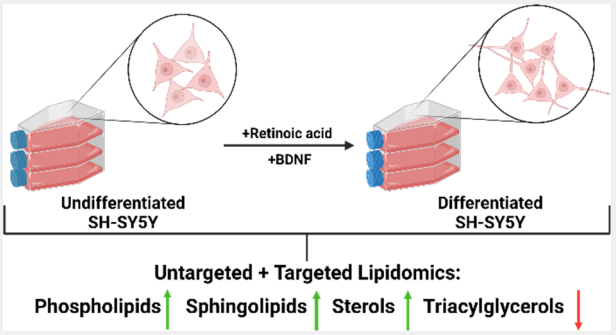

KEYWORDS: *lipidomics, SH-SY5Y, differentiation, triacylglycerides, phospholipids, sphingolipids, sterols*

INTRODUCTION

The increasing amount of neuroactive chemicals being released into the environment, combined with the susceptibility of the nervous system to the deleterious effects of xenobiotics,[1,2] warrants the evaluation of effective methods to assess the neurotoxicity of environmental contaminants. The brain is a complex structural and functional network which undergoes many changes upon exposure to neurotoxic chemicals. To better understand response mechanisms and processes that occur during these changes, various *in vivo* and *in vitro* models have been developed. A limitation of *in vivo* models, which primarily use rats, mice, zebrafish, and other nonmammalian organisms, is that they might not recapitulate mechanisms specific to humans due to differences in gene expression or regulatory mechanisms that differ in these organisms.[3,4] For this reason, various *in vitro* models using human cell lines have been pursued commonly. The human neuroblastoma cell line SH-SY5Y has been widely used as an *in vitro* model[5] to study potential neurotoxic effects of environmental contaminants and xenobiotics[6,7] and various neurological conditions such as neurotrauma,[8] neurotoxicity,[9] neurodegeneration[10] and relevant neurodegenerative diseases.[11,12]

Strong evidence exists that the developing brain is most vulnerable to toxic chemical exposure when neuronal differentiation occurs in the central nervous system, during which mature neurons form along with an interconnected network of cells capable of processing a conglomerate of information.[13] In this regard, the use of SH-SY5Y cells as an *in vitro* model to assess the neurotoxic effects of xenobiotics is advantageous because these cells can be cultured for an extended period and can be differentiated into mature neuron-like cells on a need basis. The differentiation can be achieved through treatment

Received: March 27, 2023
Revised: May 25, 2023
Accepted: May 26, 2023
Published: June 8, 2023

https://doi.org/10.1021/envhealth.3c00022
Environ. Health 2023, 1, 110−120

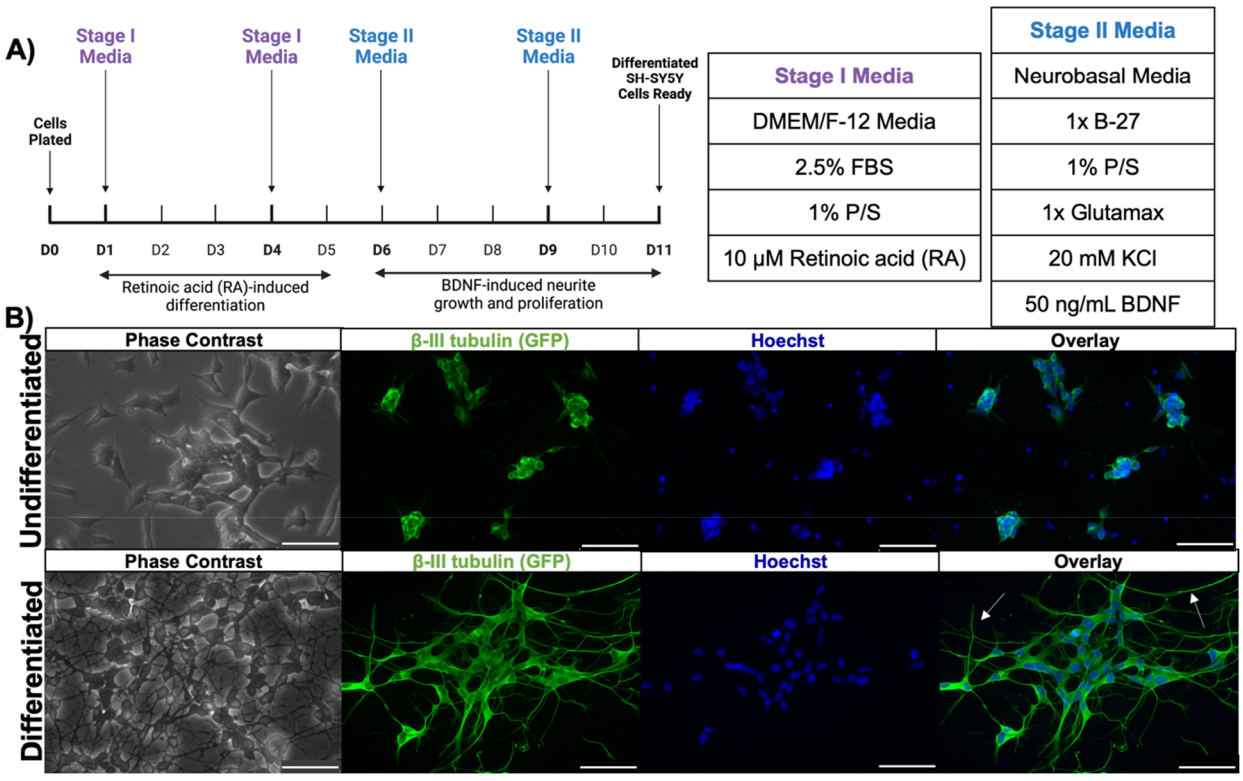

Figure 1. Timeline and reagents used in neuronal differentiation and imaging of differentiated and undifferentiated cells. (A) Timeline and table of reagents used in the differentiation of SH-SY5Y cells. Undifferentiated cells were plated in a complete growth medium containing 10% FBS overnight. Cells were then incubated for 5 days using Stage I media which contained 10 μM RA, followed by Stage II media containing 50 ng/mL BDNF for an additional 5 days. (B) Phase contrast and fluorescence microscopy images of undifferentiated and differentiated SH-SY5Y cells. Cells were stained with anti β-III tubulin and Hoechst (scale bar = 75 μm).

with different chemicals such as retinoic acid (RA), phorbol esters, and dibutyryl cyclic AMP, most commonly through the use of RA.[14]

The various mechanisms of differentiation can be used to obtain specific neuron subtypes such as adrenergic, cholinergic, and dopaminergic neurons.[15,16] RA can inhibit cell growth and promote cellular differentiation by activating the phosphatidylinositol 3-kinase/Akt signaling pathway and the upregulation of the antiapoptotic Bcl-2 protein.[17] RA also activates the transcription of many genes, cell signaling molecules, structural proteins, enzymes, and cell surface receptors such as nuclear factor κB (NFκB), microtubule-associated protein 2 (MAP2), and neurogenin 1, among others.[18] Morphologically, differentiated cells vary from undifferentiated cells as differentiated cells do not form clusters, have a pyramidal-shaped cell body with extended neurite-like structures similar to dendrites and axons, and can no longer proliferate.[19] Several markers are used to confirm differentiated SH-SY5Y cells. These include β-III tubulin, growth-associated protein 43 (GAP-43), and Tau.[20] β-III tubulin is one of the earliest neuron-associated cytoskeletal marker proteins and is necessary for morphological changes that occur during differentiation;[21−23] hence, it is extensively used to study the differentiation process.

One challenge that can confound the interpretation of results obtained from the SH-SY5Y *in vitro* cell model is the gap in knowledge on molecular changes that occur as cells are differentiated into neuron-like cells. A complete categorization of these changes is critical for the utilization of the SH-SY5Y *in vitro* cell model to study how neurons might be affected upon exposure to toxic environmental contaminants. The SH-SY5Y cells have been used for environmental neurotoxicity experiments where almost half of the studies used undifferentiated neuroblastoma cells. In these studies, several end point measurements have been used to assess the toxicity of contaminants in these cell lines, including cell viability readouts (e.g., cellular metabolic activities), cytotoxicity readouts (e.g., lactate dehydrogenase release assay, annexin V/propidium iodide staining and chromatin condensation) and measurement of acetylcholine esterase activity (reviewed in ref 6). As such, it is critical to fully understand the molecular changes that occur during differentiation to properly study neurotoxicity in response to various environmental exposures.

Even though brain development has been widely studied anatomically, cellular and molecular differences that occur during neuronal differentiation have not been fully established in the SH-SY5Y cell model.[24] Several studies have reported changes in gene expression,[25−28] proteome,[29] and other epigenetic changes[30] during the differentiation of SH-SY5Y cells. Neuronal membranes are composed of various lipid species such as glycerolipids, sterols, glycosphingolipids, and sphingomyelin-.[31] Sphingolipids and sterols have been known to play critical roles in neuronal differentiation.[32] L-Serine, specifically, is an essential amino acid for the neurodevelopment and survival of cultured neurons as a precursor in sphingolipid biosynthesis.[33] Along these lines, sphingolipids and cholesterol can form distinct membrane macrodomains called lipid rafts that are involved in cellular signaling processes related to proper cellular development and neuronal survival.[32,34] Compared to the undifferentiated state, differentiation induces a decrease in proteins involved in fatty acid

https://doi.org/10.1021/envhealth.3c00022
Environ. Health 2023, 1, 110−120

metabolism, phosphatidylserine (PS) aminotransferase, and lipid raft linker gene 1. Differentiation also increases expression levels of several proteins such as proteins involved in cholesterol metabolism,[35] lyso-phosphatidylglycerol acetyltransferase, glucoceramidase, and CDP-diacylglycerol inositol phosphatidyltransferase and several genes including stearoyl-CoA desaturase and acetyl-CoA synthase 1/2[26] in SH-SY5Y cells. However, no study has comprehensively investigated the changes in the cellular lipidome during neuronal differentiation.

Given previous studies on the regulation of the lipidome during different cell cycle stages[36,37] and morphological changes that occur during differentiation, we envisioned that lipids might be tightly regulated during this process. Previous studies have conducted lipidomics during cellular differentiation of other cell types such as stem cells, among others;[38,39] however, changes in the cellular lipidome during neuronal differentiation is understudied. In this work, we aim to elucidate the changes in the cellular lipidome during the differentiation of SH-SY5Y neuroblastoma cells into neuron-like cells achieved by RA treatment using untargeted and targeted lipidomics. We show that there are global differences between the cellular lipidome of undifferentiated and differentiated SH-SY5Y cells. Our results clearly demonstrate that the cellular lipidome is regulated during differentiation, highlighting changes in sterol, sphingolipid and triacylglycerol species. We believe that these lipidomic changes establish an important consideration while utilizing SH-SY5Y cells as an *in vitro* model to study neuronal toxicity of environmental contaminants and obtain a better understanding of the lipid-related changes that occur during differentiation.

RESULTS AND DISCUSSION

SH-SY5Y Cell Line as a Model System to Study Differentiation

The SH-SY5Y neuroblastoma cell line is commonly used to study neurological pathologies and has been a widely accepted model used to study neuronal differentiation.[5,6,11,40] These cells are clones derived from the parental neuroblastoma cell line which was originally generated from a bone marrow biopsy.[41] In this study, we investigated the changes in the cellular lipidome during the differentiation of SH-SY5Y cells using targeted and untargeted lipidomics. We differentiated these cells using previously published protocols.[5,42] Briefly, undifferentiated SH-SY5Y cells were plated using a complete growth medium containing 10% fetal bovine serum (FBS) and were allowed to attach overnight. The cells were then treated for 5 days with media containing reduced serum and 10 μM RA (Stage I media, Figure 1A). RA was added to the cells in order to induce cell cycle arrest to drive neuronal differentiation.[14] After 5 days of treatment with Stage I media, the cells were grown in a neurobasal growth medium containing 50 ng/mL brain-derived neurotrophic factor (BDNF) for an additional 5 days (Stage II media, Figure 1A). BDNF is involved in the maintenance of cortical neurons and its intracellular signaling is important for neuronal survival, morphogenesis, and plasticity.[43] This procedure results in differentiated neuron-like cells which exhibit a cholinergic type. Since differentiation is accompanied by drastic morphological changes, cells were imaged using phase contrast and fluorescence microscopy to study the morphological differences between undifferentiated and differentiated SH-SY5Y cells (Figure 1B). Para-formaldehyde-fixed differentiated and undifferentiated cells were stained with anti β-III tubulin[44] and Hoescht (a nuclei stain). Similar to the observations in previous publications,[5] undifferentiated cells tend to cluster together and have very short projections (Figure 1B). On the other hand, differentiated cells exhibited long and extensive branched neurite-like structures (Figure 1B, marked with white arrows), positive for β-III tubulin. These results are consistent with previous studies that show a marked increase in β-III tubulin in neurite-like structures in differentiated cells.[45,46]

Untargeted Lipidomics Highlights the Changes in the Cellular Lipidome during the Differentiation of SH-SY5Y Cells to Neuronal-Like Cells

For lipidomic analysis, differentiated and undifferentiated samples (n = 5) were prepared and analyzed using LC−MS in positive and negative electrospray ionization mode (+ESI and −ESI) as we previously described.[47] Scheme 1 shows the lipidomics workflow for both untargeted and targeted analysis.

Scheme 1. Scheme Describing Targeted (Red) and Untargeted (Yellow) Workflow for Lipidomic Analysis in Differentiated and Undifferentiated SH-SY5Y Cells[a]

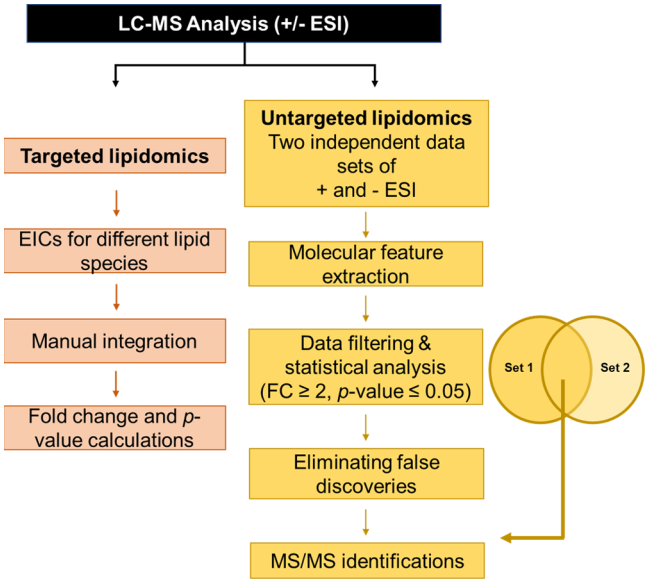

[a]Samples (n = 5 replicates) were run in positive and negative mode (+ESI and −ESI) twice in each mode to remove any false positives. For targeted analysis, peak areas in extracted ion chromatograms (EICs) were manually integrated. The fold changes and p-values were calculated. For untargeted analysis, raw data obtained from LC−MS analysis were imported into MassHunter Profinder (Agilent Technologies), where unique features were extracted and peak alignment was carried out based on m/z, retention time, isotopic ratio, and grouping of different adducts. Data from Profinder were then imported into MassHunter Mass Profiler Professional (MPP, Agilent Technologies), where species were filtered based on the frequency with which they were present in each sample. Species that were present in both independent data sets were used for further analysis. Statistical significance was determined using the student's t-test and features with $p \geq 0.05$ were eliminated and the fold change (FC) ≥ 2 of the remaining species were subsequently calculated as [Abundance$_{\text{differentiated}}$]/[Abundance$_{\text{undifferentiated}}$] for each species. To identify lipid candidates, m/z's obtained were searched in LipidMaps.[48] Known lipid standards or representative lipids were purchased for the candidate lipids to confirm MS/MS fragmentation patterns.

https://doi.org/10.1021/envhealth.3c00022
Environ. Health 2023, 1, 110−120

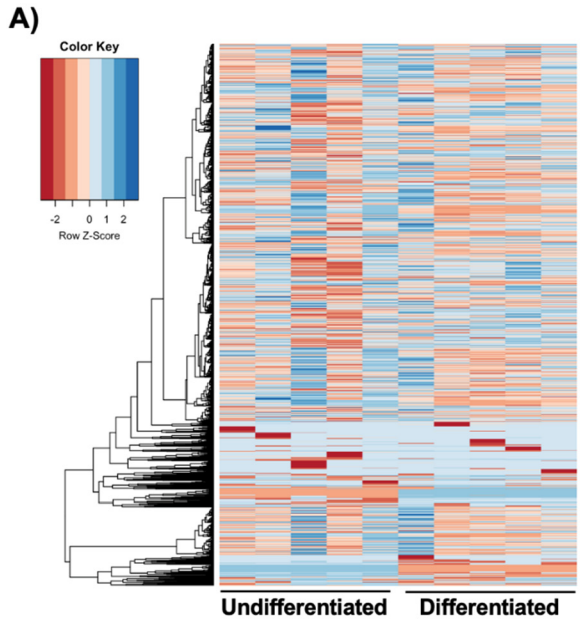

Lipid Class	m/z
Phospholipids	692.5263, 720.5594, 728.5268, 739.5731, 746.5733, 747.5264, 750.5140, 800.6146, 806.5734, 816.5934, 820.6218, 822.5355, 832.5855
Glycerolipids	400.3423, 860.7655, 892.7413, 920.7733, 922.7898, 927.7468, 946.7814, 948.8016, 970.7847, 998.8105
Sterols	343.2965, 381.2521, 409.2836, 426.3586, 429.3745
Sphingolipids	592.5698, 674.6479, 675.5458, 728.5634

Figure 2. Hierarchal clustering of molecular extraction features obtained and lipid classes identified using untargeted lipidomics. (A) Hierarchal clustering analysis of the lipidome during cellular differentiation was performed. The scaled abundances are represented as a heat map and individual samples were grouped based on the abundance of detected ions found in the untargeted analysis. (B) Pie chart describing the amount of MS/MS identifications separated via lipid class in terms of percentage of the total identified lipids along with a table of the *m/z* identified from each class. Phospholipids and glycerolipids were the most abundant species identified via MS/MS which had statistically significant changes in differentiated vs undifferentiated SH-SY5Y cells. Sterols and sphingolipids were also identified via MS/MS. See Table 1 for the identifications of each species along with the method of identification, *m/z*, fold changes (FC), and *p*-values. Table S1 contains the information shown in Table 1 along with some additional information such as the MS/MS fragments obtained and searched in the databases, and retention times (R_t).

For untargeted analysis, raw data were imported into Profinder (Agilent Technologies) software where peaks were aligned based on their *m/z*, adducts, retention time, and isotopic ratio. Data from Profinder were then analyzed in MassHunter Mass Profiler Professional (MPP, Agilent Technologies). Using these data, we first produced a heatmap by hierarchical clustering (Figure 2A). Overall, we observed distinct clustering of differentiated and undifferentiated cells without any prior statistical analysis or filtering, suggesting that major compositional differences in the lipidome occur during differentiation. To identify lipid species that showed significant differences between differentiated and undifferentiated cells, features detected were first filtered based on the frequency they were present in different samples. The features that were not present in all biological replicates in two independent data sets were excluded from further analysis. The fold change (FC) of the resulting features was analyzed. The features that showed a significant difference of FC $\geq$ 2 (*p*-value $\leq$0.05, student's *t*-test) in two independent profiling experiments were identified. These species were selected for identification (Scheme 1).

A total of 44 species (37 in +ESI and 7 in −ESI) significantly changed during differentiation (Table 1). To identify lipid candidates, *m/z* values obtained were searched in LipidMaps.[48] Subsequent lipid identifications were done using MS/MS, via fragmentation match to representative lipid species and two different databases (MyCompound ID[49] and Human Metabolome Database [HMDB][50]) to search for fragments. Overall, of the 44 statistically significant species that showed a FC $\geq$ 2, 32 species were identified through a comparison of the fragmentation of a representative lipid species or the database searches. First, we conducted MS/MS experimenting between the hits and a representative lipid from the predicted family and compared fragmentation patterns. We identified 13 out of the 44 species shown in green in Table 1 (for detailed information see Supporting Information document and Table S1 which reports retention times (R_t), MS/MS fragments identified using a representative lipid species along with MS/MS fragments input in the databases). For the rest of the species, MS/MS fragments were searched on each database by inputting *m/z* of the fragments obtained, along with their relative intensities, and allowed ppm error (±15 ppm). Based on the information provided, MyCompound ID searches the MS/MS fragments and intensities given against a library of over 8,000 human metabolites from an MS/MS spectrum and will give putative compounds along with a fit score out of 1.000. A fit score greater than 0.700 suggests an assignment that is highly likely correct.[51] HMDB compares the MS/MS fragments and intensities given against a library of over 220,000 metabolites and will provide possible identifications along with the ppm error of each match. Using these two databases, 19 additional species were identified (listed in red for MyCompound ID, and blue for HMDB, respectively, Table 1). Figure 2B shows the different classes of lipids identified via a percentage along with the *m/z* that belongs to each lipid class. The majority of the species identified using untargeted analysis belonged to the phospholipid family (i.e., 41%) and glycerolipids, predominantly triacylglycerols (TAGs) (i.e., 31%). Sphingolipids and sterols were the other lipid families identified using untargeted lipidomics workflow. In differentiated cells, sterols, phosphatidylcholines (PCs), phosphatidylserines (PSs), phosphatidylglycerols (PGs), and phosphatidylethanolamines (PEs), a ceramide (Cer) and sphingomyelin (SM) showed accumulations ranging from 1.8 to 14.9-fold as compared to their undifferentiated counterpart. We also observed that some sphingolipids and TAGs are depleted

https://doi.org/10.1021/envhealth.3c00022
Environ. Health 2023, 1, 110−120

Table 1. Identifications of Lipid Species Using MS/MS Fragmentation or Database Searches[a]

	m/z	Identifications	Fold Change	p-value
POSITIVE MODE IONIZATION (+ESI)	343.2965	ST 24:1;O2	3.0	*
	381.2521	ST 22:1;O5	2.5	*
	400.3423	MG 20:2	2.2	**
	409.2836	ST 24:1;O2	2.4	*
	413.2726	N/A	0.3	***
	426.3586	ST 29:4;O	11.6	***
	429.3745	ST 29:2;O2 ST 29:2;O2	14.9	***
	469.3671	N/A	11.5	***
	504.4212	N/A	0.4	**
	629.5534	N/A	2.3	***
	630.5509	N/A	2.5	*
	675.5458	SM 32:1	2.4	***
	689.5604	N/A	0.1	***
	692.5263	PC 29:0	0.3	***
	697.5247	N/A	2.7	***
	702.5463	N/A	2.6	**
	720.5594	PC 31:0 PC31:0	0.2	**
	728.5634	SM d18:1/18:0	3.4	**
	739.5731	PC 30:2	0.4	**
	746.5733	PC 33:1 PC 33:1	0.2	***
	750.5140	PC 34:6 PC 34:6	1.8	***
	800.6146	PC 37:2 PC 37:2	0.2	**
	806.5734	PC 38:6	0.3	***
	816.5934	PC 40:6	0.1	***
	820.6218	PC 22:4/P-18:1	0.1	***
	832.5885	PC 40:7 PC 40:7	0.2	***
	860.7655	TAG (51:3)	0.2	***
	892.7413	TAG (54:8)	0.4	***
	914.5174	N/A	2.8	**
	920.7733	TAG (56:8)	0.4	***
	922.7898	TAG (56:7)	0.4	***
	927.7468	TG 58:10	0.3	***
	946.7814	TAG (58:9)	0.4	***
	948.8016	TAG (58:8)	0.4	**
	953.9045	N/A	0.4	**
	970.7847	TAG (60:11)	0.3	***
	998.8105	TAG (62:11)	0.2	***
NEGATIE MODE IONIZATION (-ESI)	592.5698	Cer (d18:1/20:0)	3.5	***
	674.6479	Cer (d20:1/24:1)	0.4	**
	728.5268	PE (17:1,18:1)	4.1	**
	747.5264	PG (16:0,18:1)	3.7	**
	770.5369	N/A	4.0	**
	800.5471	N/A	2.9	**
	822.5355	PS(19:1,20:4)	3.9	***

[a]Species were identified using two different methods: based on their MS/MS fragmentation and comparing their fragments to known fragments of a standard lipid of the representative class (labeled in green) or searching their fragments and relative intensities obtained using MS/MS in two different databases − MyCompound ID (labeled in red) and Human Metabolome Database (HMDB, labeled in blue). The table shows *m/z*, and color-coded identification, along with their respective fold changes (FC) and *p*-values. **p*-value ≤0.05; ***p*-value ≤0.01; ****p*-value ≤0.001.

approximately 2-fold or more in differentiated cells (FC ≤ 0.4) compared to undifferentiated cells.

Sterols are an important class of lipids that are highly abundant in brain tissue. A recent study on cholesterol biosynthesis and the biosynthesis of other sterols in developing neurons found that developing neurons have significantly higher levels of both cholesterol and sterol derivatives per cell compared to astrocytes,[52] consistent with the accumulation of sterols that we observe in differentiated cells. This is likely because cholesterol is necessary for the formation of synapses and dendrites and axonal guidance.[53] It has been shown that changes in sterol levels have occurred in response to the exposure of various environmental contaminants, including per- and polyfluorinated alkyl substances (PFAS),[54] suggesting these contaminants might affect the survival of differentiated neurons via cholesterol metabolism-dependent mechanisms.

Since phospholipids are a major component of cellular membranes, it has been suggested that they play an important role in membrane biosynthesis that occurs during neuronal differentiation.[31] PCs, specifically, account for approximately 58% of all phospholipid species present in mammalian membranes.[55] For this reason, most studies on the changes in phospholipids during neuronal differentiation have only focused on PCs and not on the other phospholipid species (such as PEs, PGs, and PSs). These studies have found that PC biosynthesis is upregulated during neuronal differentiation[31,56] which differs from our results that show the depletion of long-chained PCs in differentiated cells. It is possible that PCs are used up for the biosynthesis of other phospholipid species accumulate in differentiated cells, consistent with our data.

As we discussed earlier, since sphingolipids play an important role in neuronal differentiation, it is expected that some sphingolipid species such as ceramides can be upregulated in differentiated cells, consistent with our untargeted lipidomics results (Table 1). Sphingolipids, such as ceramide and sphingomyelin, are involved in the process of axonal projection and outgrowth.[57] Studies have shown that inhibition of ceramide synthesis will lead to a buildup of ceramide precursors (i.e., sphingosine and sphinganine) which causes a decrease in axonal growth during neuronal development.[58] Similarly, inhibition of serine palmitoyltransferase, the first step in sphingolipid biosynthesis, inhibits dendritic development and survival indicating the importance of *de novo* sphingolipid biosynthesis.[59]

Lastly, no previous studies have investigated the levels of glycerolipids during neuronal differentiation. We found that TAGs are significantly depleted in differentiated cells ($p \leq 0.05$) with longer-chained TAGs and polyunsaturated ones being prominent (Table 1). Studies have shown decreased activity of Δ4 desaturase, in neuroblastoma cells[60] which might explain the lower levels of polyunsaturated TAGs in differentiated cells relative to undifferentiated cells. A study conducted on postnatal rats compared the levels of cholesterol esters and TAGs in glial vs neurons and found that TAG levels were much lower in neurons compared to the glial cells.[61] TAGs play lipid storage roles in neuronal lipid metabolism[62] similar to other tissues. Hence, it is possible that they are depleted in differentiated cells due to the breakdown of TAGs in order to synthesize more lipids, such as phospholipids or sphingolipids, which are necessary for neuronal differentiation and axonal projection. A study conducted in rat brains found that TAG levels were the lowest in younger rats during central nervous system development and increased to their highest level in adults. The authors also looked at the metabolism of a ^{14}C-labeled TAG and found that after 6 h it was metabolized almost fully into the major phospholipids of the brain such as PCs, PEs, PSs, and PIs.[63]

https://doi.org/10.1021/envhealth.3c00022
Environ. Health 2023, 1, 110−120

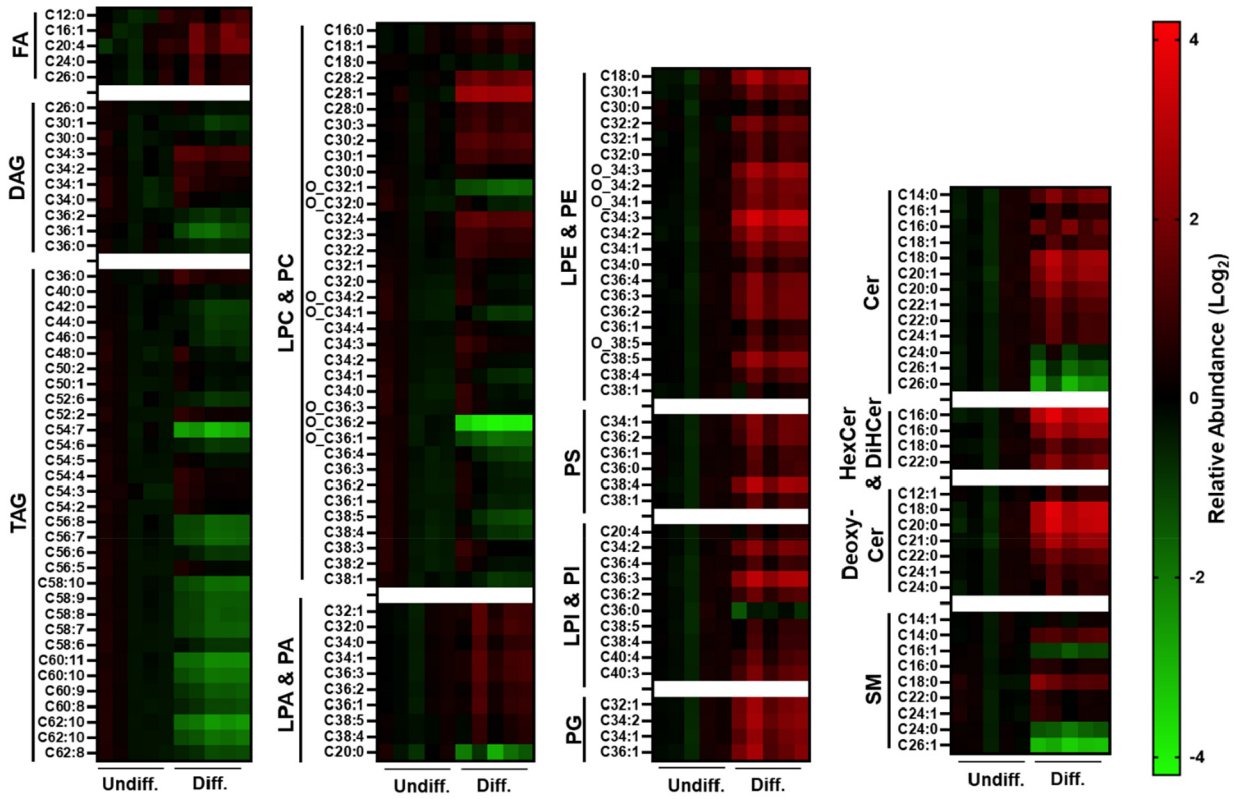

Figure 3. Targeted lipidomics highlights the changes in phospholipids, sphingolipids, and glycerolipids during neuronal differentiation. Targeted lipids include phosphatidylethanolamines (PEs), phosphatidylserines (PSs), phosphatidylinositols (PIs), phosphatidylglycerols (PGs), phosphatidylcholines (PCs), phosphatidic acids (PAs), diacylglycerols (DAGs), triacylglycerols (TAGs), ceramides (Cers), dihydroceramides (DiHCers), hexosylceramides (HexCers), deoxyceramides (DeoxyCers), sphingomyelins (SMs), and fatty acids (FAs). The red-to-green heat map shows the $\log_2$ relative abundances comparing undifferentiated to differentiated cells. All individual abundances of both undifferentiated and differentiated species were normalized to the average abundance of the undifferentiated condition.

Targeted Lipidomics Supports the Accumulation of Phospholipids and Sphingolipids and the Depletion of Triacylglycerols during Differentiation

We next conducted a targeted analysis of various lipid classes with different acyl chain lengths and degrees of unsaturation based on the hits from the untargeted analysis. For this analysis, the m/z values of each lipid species were extracted, and the corresponding peaks were manually integrated (see Figure 3 for a heatmap representation of the relative abundances of the targeted lipid species for differentiated and undifferentiated cells). Targeted lipid classes included fatty acids (FAs), PEs, PSs, PIs, PGs, PCs, phosphatidic acids (PAs), diacylglycerols (DAGs), TAGs, Cers, DiHCers, HexCers, and SMs. Prior to calculating the relative abundances of the targeted analytes at each condition, all raw abundances were first corrected with an internal standard mix containing a nonendogenous lipid species from each class.

Most of the phospholipid species (except PCs and PAs) had significantly higher levels in differentiated cells compared to the undifferentiated cells ($p \leq 0.05$, Figure 3). Surprisingly, even though we identified multiple PC species which had decreased significantly in our untargeted analysis, we identified three ether linked PC species (O_C36:2, O_36:1, O_32:1) that were depleted in differentiated cells in our targeted analysis (Table 1 and Figure 3). The medium chain PCs modestly accumulated in differentiated cells, similar to our observations in untargered analysis, which might be linked to increased lipid demand of differentiated cells for morphological changes that occur during neuronal differentiation. The downregulation of ether-linked PCs is intriguing in this context and further studies are warranted to provide functional links to differentiation.

For the glycerolipid species that were targeted, we did not observe any significant changes in DAGs. However, TAGs were significantly downregulated in differentiated cells (Figure 3), consistent with our untargeted hits (Table 1). As we discussed earlier, the decrease in TAGs could be due to the turnover of TAGs to provide additional phospholipids needed for membrane remodeling for the morphological changes that occur during differentiation, such as elongation and formation of the axonal projections (Figure 1B). Since phospholipids are the major component of cellular membranes, it is likely that TAGs, which are primarily used for storing excess cellular lipids,[64] are being broken down in order to synthesize phospholipids needed during differentiation.

Lastly, we observed higher levels of all of Cer, HexCer, DiHCer, DeoxyCer, and some SMs in differentiated cells. Sphingolipids are essential to proper brain development and critical for the nervous system's integrity. This is because sphingolipids play a key role in the regulation of axonal growth.[65] Further, Cer and sphingosine-1-phosphate (S1P) in neural signaling and function by their ability to affect specific signaling cascades.[66] Perturbations in the sphingolipid metabolism, such as the accumulation of the sphingolipid precursors sphingosine and sphinganine in the brain have been linked to various neurological diseases.[58] It has also been

https://doi.org/10.1021/envhealth.3c00022
Environ. Health 2023, 1, 110−120

shown that depletions of Cers, SMs, and HexCers significantly reduce axonal projections, which are essential for the development of neuronal networks.[67] This is consistent with our observations where Cers, HexCers, and some SM species accumulated in differentiated cells. Various studies have also shown that sphingolipid levels are affected in response to exposure to various environmental contaminants such as persistent organic pollutants[68] and PFAS,[69] suggesting that environmental contaminants might perturb neuronal differentiation via their effect on sphingolipid metabolism.

SUMMARY AND CONCLUSIONS

To complement information from epidemiological studies that associate increased incidence of neurodevelopmental toxicities with environmental exposure to chemical contaminants, there is a need for reliable *in vitro* cell models that can provide insights into the mechanisms of neurotoxicity of chemicals. Currently, no study has been conducted to investigate the specific changes in the cellular lipidome during neuronal differentiation. Our results highlight the changes in the cellular lipidome which occur during neuronal differentiation *in vitro* using a model cell line, SH-SY5Y, using both untargeted and targeted lipidomics. We showed that TAGs are significantly depleted in differentiated neuronal cells. We also showed that phospholipids (specifically PGs, PEs, PIs, and PSs) and sphingolipids are present in differentiated cells at significantly higher levels compared to undifferentiated cells.

The significance of these results is 2-fold. First, the clear differences in the cellular lipidome between differentiated and undifferentiated SH-SY5Y cells will pave the way for a better understanding of the biochemical changes that occur in neuronal differentiation and will enable a better understanding of the molecular components of this process. In the future, studies can be conducted to reveal the functional involvement of specific lipid species that we have identified in this work for neuronal differentiation which may be critical for uncovering new targets responsible for neurological disorders. Second, we believe that the changes in the lipidome reported in this work, along with previous studies describing transcriptomic and proteomic changes, highlight the large molecular differences between differentiated and undifferentiated states. These differences may impact how cells respond to different perturbations and call for careful considerations while using these different states for various research questions. These changes may be linked to the morphological changes that occur during differentiation which require additional lipid production needed for increased membrane demand. We believe that these changes could significantly impact the biophysical properties of cellular membranes and can potentially affect the uptake of xenobiotics and their cytotoxicity.

MATERIALS AND METHODS

Materials

Human neuroblastoma epithelium (SH-SY5Y) was purchased from American Type Culture Collection (Manassas, Virginia). Dulbecco's modified Eagle's medium/nutrient mixture F-12 (DMEM/F-12), fetal bovine serum (FBS), penicillin, streptomycin, and trypsin were purchased from Corning (Corning, NY). All-*trans* retinoic acid (RA) was purchased from Cayman Chemical Company (Ann Arbor, MI). Gibco neurobasal medium, Gibco B-27 supplement, Hoechst 33342, Alexa Fluor 488 antimouse, M-PER Mammalian Protein Extraction Reagent, Pierce protease inhibitor mini tablets, EDTA-free and GlutaMAX supplement were purchased from Fisher Scientific (Hampton, NH). Coomassie protein assay reagent and albumin standard for the Bradford assay kit were purchased from Thermo Fisher Scientific (Waltham, MA). Brain-derived neurotrophic factor (BDNF) was purchased from Prospec (Ness-Ziona, Israel). KCl, Tween 20, and 37% paraformaldehyde solution were obtained from VWR International (Radnor, PA). Poly-D-lysine solution (1 mg/mL) was purchased from MilliporeSigma (Burlington, MA). TritonX-100, bovine serum albumin, and monoclonal anti-β-tubulin isotype III were obtained from Sigma-Aldrich (St. Louis, MO). Prolong Gold antifade reagent was purchased from Invitrogen (Waltham, MA). C17:0 sphingomyelin, d^9 oleic acid, C17:0 ceramide, C39:0 TAG, C12:0 deoxyceramide, and C18:0/C18:0 phosphatidylcholine-d^{70} were purchased from Avanti Polar Lipids (Alabaster, AL). Liquid chromatography−mass spectrometry (LC−MS) columns and guard columns were obtained from Phenomenex (Torrence, CA). Mass Hunter Qualitative Analysis (version 06.00), MassHunter Profinder (version B.06.00), and MassHunter Mass Profiler Professional (version B12.6.1) were obtained from Agilent Technologies (Santa Clara, CA). LC−MS grade methanol and HPLC grade isopropanol were purchased from EMD Millipore (Charlotte, NC). HPLC-grade chloroform was purchased from Honeywell (Charlotte, NC).

Preparation of Stock Solutions

A 5 mM stock of all-*trans* retinoic acid was prepared in 95% ethanol and stored in an amber vial at 4 °C. It was freshly added at a 1:500 dilution into Stage I media prior to use. A 10 μg/mL stock of brain-derived neurotrophic factor was prepared by in 1 mL of neurobasal medium supplemented with B-27 supplement and stored at −80 °C. It was added to Stage II media at a 1:200 dilution. A 1 M stock of KCl was added to Stage II media at a 1:50 dilution.

0.1% TritonX solution in PBS was prepared by adding 50 μL of 20% TritonX (in PBS) to 10 mL of PBS and stored at room temperature until used. 0.1% Tween 20 solution in PBS was prepared by adding 10 μL of Tween 20 to 10 mL of PBS and stored at room temperature until used. Hoechst solution was prepared in PBS and stored at 4 °C. Immediately prior to use 1 μL of the solution was added to 10 mL of PBS to make a 0.1 μg/mL solution (1:10,000).

Cell Culture

SH-SY5Y cells were grown in Dulbecco's modified Eagle's medium/nutrient mixture F-12 (DMEM/F-12) supplemented with L-glutamine and 15 mM HEPES. The medium was supplemented with 10% (v/v) fetal bovine serum (FBS) and 1% (v/v) penicillin-streptomycin (P/S). Cells were grown at 37 °C and in 5% CO_2.

Differentiation of SH-SY5Y Cells

Undifferentiated cells were seeded in basic growth media to a ∼80% confluency (e.g., 1 × 10^6 cells per 10 cm Petri dish and ∼50,000 cells per well in a 24-well plate) and allowed to attach for 24 h (day 0). For imaging, cells were plated onto glass cover slips placed in a 24-well plate coated with poly-D-lysine according to the manufacturer's instructions. To induce differentiation, cells were treated using an established protocol.[5] After 24 h, the media were changed to Stage I media which were composed of DMEM/F-12 supplemented with 2.5% FBS, 1% P/S, and 10 μM retinoic acid (RA) (day 1). RA was added to the cells in order to induce cell cycle arrest to drive neuronal differentiation.[14] On day 4, the media were replaced with fresh Stage I media. On day 6, the medium was changed to Stage II medium which was composed of Neurobasal medium supplemented with 50 ng/mL brain-derived neurotrophic factor (BDNF), 20 mM KCl, B-27 supplement, GlutaMAX, and 1% P/S. BDNF is important for neuronal survival, morphogenesis, and plasticity, making it necessary for cells to undergo neuronal differentiation *in vitro*.[43] This procedure results in differentiated neuron-like cells which exhibit a cholinergic type. On day 9, the media were replaced with fresh stage II media. Cells were then ready for collection on day 11.

Immunofluorescence

SH-SY5Y cells were fixed with 4% paraformaldehyde dissolved in PBS. The solution was gently aspirated from the cover slips and

https://doi.org/10.1021/envhealth.3c00022
Environ. Health 2023, 1, 110−120

subsequently washed with 200 μL of PBS for 1 min. PBS was removed and 100 μL of PBS-Triton (0.1%) for permeabilization was added and incubated for 10 min at room temperature. The solution was removed, and the cover slips were blocked with 2% bovine serum albumin dissolved in 1% Triton X in PBS for 1 h at room temperature. Cover slips were washed with 200 μL of 0.1% Tween 20 in PBS for 5 min. The solution was removed and incubated with 100 μL of the primary antibody (β-III tubulin, 1:400) diluted in 1% bovine serum albumin dissolved in 0.1% TritonX in PBS overnight at 4 °C. The cover slips were washed with 0.1% Tween 20 in PBS prior to 100 μL secondary antibody (Alexa Fluor 488 antimouse, 1:1000) incubation diluted in 1% bovine serum albumin dissolved in 0.1% TritonX in PBS for 1 h at room temperature. The solution was removed, and cover slips were washed with 0.1% Tween 20 in PBS. 100 μL of Hoechst (1:10,000) diluted in PBS was added to each cover slip and incubated for 10 min at room temperature protected by light. The solution was removed, and cover slips were washed with 0.1% Tween 20 in PBS prior to mounting using Prolong Gold Antifade Reagent.

Cell Collection and Lipid Extraction

Frozen cell pellets were resuspended in 1 mL of cold PBS, and a 30 μL aliquot of the cell suspension was then taken and mixed with an equal volume of lysis buffer and incubated on ice for an hour. The protein concentration of each sample was determined using a Bradford assay. The cell pellet containing the remaining 970 μL was transferred to a glass Dounce homogenizer along with 1 mL of cold methanol and 2 mL of cold chloroform. Cells were homogenized (30x) and subsequently centrifuged at 4 °C, 500*g*, for 10 min to separate the aqueous and organic layers. The organic layer was then carefully removed and transferred to a 1 dram glass vial. The chloroform layer was then dried under N_2 gas. The dried lipid extracts were stored in freezer until analysis. Prior to analysis, samples were normalized based on their protein content and resuspended in spiked chloroform ≥150 μL. C17:0 sphingomyelin, d^9 oleic acid, C17:0 ceramide, C39:0 TAG, C12:0 deoxyceramide, and C18:0 phosphatidylcholine-d^{70} were used as internal standards.

Total Protein Concentration and Sample Normalization

Cells were lysed in lysis buffer containing M-PER Mammalian Protein Extraction Reagent supplemented with a protease inhibitor mini tablet. Cells were lysed for an hour and the total protein concentration of cell lysates was determined by mixing 20 μL of the cell lysate and 1 mL Bradford solution. The solution was vortexed and incubated at room temperature for 10−15 min. The protein concentration was determined by an absorbance measurement at 595 nm. A calibration curve was prepared by using known concentrations of bovine serum albumin. Cellular lipid extracts were then normalized by resuspending the dried samples in calculated volumes of spiked chloroform based on total protein content.

LC−MS Acquisition

LC−MS analyses were carried out using an Agilent 1260 HPLC in tandem with an Agilent 6530 Jet Stream ESI-QToF-MS system. Reversed-phase chromatography was used for separation prior to mass analysis. A Gemini C18 reversed-phase column (5 μm, 4.6 mm × 50 mm) with a C18 reversed-phase guard cartridge was used for negative mode. A Luna C5 reversed-phase column (5 μm, 4.6 mm × 50 mm) with a C5 reversed-phase guard cartridge was used for positive mode. Mobile phase A was composed of 95:5 water:methanol (v/v) and mobile phase B was composed of 60:35:5 isopropanol:methanol:water (v/v) for both positive and negative modes. For improved negative ion detection, mobile phases were supplemented with 0.1% ammonium hydroxide (w/v). For improved positive ion detection, mobile phases were supplemented with 0.1% formic acid (v/v) and 5 mM ammonium formate. The flow rate was 0.1 mL/min for the first 5 min followed by 0.5 mL/min for the remainder of the analysis. The gradient began after 5 min from 0% B and increased to 100% B over 60 min. It was then held at 100% B for 7 min. The column was then equilibrated at 0% B for 8 min. A DualJSI fitted electrospray ionization (ESI) source was used. The capillary voltage was set to 3500 V and the fragmentor voltage was set to 175 V. The drying gas temperature was set to 350 °C with a flow rate of 12 L/min. All data were collected using an m/z range of 50−1700 in an extended dynamic range.

Targeted Lipidomics Data Analysis

Representative lipid species were targeted by extracting the corresponding m/z for each ion in MassHunter Qualitative Analysis software. Peak areas for each ion were integrated and represented as abundance. Relative abundances used in heatmaps for the differentiated samples (n = 5) were normalized to the undifferentiated cells by dividing the average abundance of a lipid species in the undifferentiated cells by the individual abundances of undifferentiated samples.

Untargeted Lipidomics Data Analysis

Five biological replicates of differentiated and undifferentiated cells were used for an independent profiling experiment in positive and negative electrospray ionization modes. Two independent profiling experiments were performed. Raw data were imported into MassHunter Profinder, where unique features were extracted and peak alignment was carried out based on m/z, retention time, isotopic ratio, and grouping of different adducts. Data from Profinder were then imported into MassHunter Mass Profiler Professional, where species were filtered based on the frequency with which they appeared in each sample. Statistical significance was determined using the student's t-test and features with p-value ≥0.05 were eliminated and the fold changes of the remaining species were subsequently calculated as $[\text{Abundance}_{\text{differentiated}}]/[\text{Abundance}_{\text{undifferentiated}}]$ for each species. Species that showed reproducible changes in the two independent profiling experiments with an average fold change ≥2 and p-value ≤0.05 were identified via MS/MS analysis.

Lipid Identifications

Lipid standards (or lipids belonging to the same lipid families) were purchased for comparison of fragmentation patterns with the features identified. MS/MS data were collected similarly to the LC−MS Acquisition section, except data acquisition was in 4 GHz high-resolution mode. Fragments were observed at collision energies of 15, 35, and 55 eV. The MS/MS fragmentation patterns of the species of interest and candidate lipids were compared. Fragments observed are provided in the Supporting Information. Lipids that were not initially identified by comparing fragmentation patterns were then identified by comparing the suggested identification from LipidMaps and the obtained MS/MS fragments, whether it was positive or negative ions, along with their relative intensities, and ppm error desired (we chose identifications with a ppm error ≤15) on 2 separate databases: MyCompound ID[49] and Human Metabolome Database (HMDB).[50] Fragments that were searched on the databases are listed in the Supporting Information (Table S1).

■ ASSOCIATED CONTENT

Supporting Information

The Supporting Information is available free of charge at https://pubs.acs.org/doi/10.1021/envhealth.3c00022.

Supplemental identification of species from untargeted lipidomic profiling; table of statistically significant species identified via MS/MS or database search along with their corresponding m/z, retention time (R_t), fold change, and p-value (PDF)

■ AUTHOR INFORMATION

Corresponding Author

G. Ekin Atilla-Gokcumen − *Department of Chemistry, University at Buffalo, The State University of New York (SUNY), Buffalo, New York 14260, United States;* orcid.org/0000-0002-7132-3873; Email: ekinatil@buffalo.edu

https://doi.org/10.1021/envhealth.3c00022
Environ. Health 2023, 1, 110−120

Authors

Michelle Camdzic − *Department of Chemistry, University at Buffalo, The State University of New York (SUNY), Buffalo, New York 14260, United States;* orcid.org/0000-0002-9928-1070

Diana S. Aga − *Department of Chemistry, University at Buffalo, The State University of New York (SUNY), Buffalo, New York 14260, United States;* orcid.org/0000-0001-6512-7713

Complete contact information is available at: https://pubs.acs.org/10.1021/envhealth.3c00022

Notes

The authors declare no competing financial interest.

■ ACKNOWLEDGMENTS

The authors gratefully acknowledge the support from the National Science Foundation (CBET-2112201). Any opinions, findings, conclusions, and recommendations expressed in this publication are those of the author(s) and do not necessarily reflect the view of the National Science Foundation.

■ REFERENCES

(1) Grandjean, P.; Landrigan, P. J. Developmental neurotoxicity of industrial chemicals. *Lancet* **2006**, *368* (9553), 2167−2178.

(2) Grandjean, P. *Only one chance: how environmental pollution impairs brain development--and how to protect the brains of the next generation*; Oxford University Press, 2015.

(3) Otey, C. A.; Boukhelifa, M.; Maness, P. B35 neuroblastoma cells: an easily transfected, cultured cell model of central nervous system neurons. *Methods Cell Biol.* **2003**, *71*, 287−304.

(4) LePage, K. T.; Dickey, R. W.; Gerwick, W. H.; Jester, E. L.; Murray, T. F. On the use of neuro-2a neuroblastoma cells versus intact neurons in primary culture for neurotoxicity studies. *Crit. Rev. Neurobiol.* **2005**, *17* (1), 27−50.

(5) Dravid, A.; Raos, B.; Svirskis, D.; O'Carroll, S. J. Optimised techniques for high-throughput screening of differentiated SH-SY5Y cells and application for neurite outgrowth assays. *Sci. Rep.* **2021**, *11* (1), 23935.

(6) Lopez-Suarez, L.; Al Awabdh, S.; Coumoul, X.; Chauvet, C. The SH-SY5Y human neuroblastoma cell line, a relevant in vitro cell model for investigating neurotoxicology in human: focus on organic pollutants. *Neurotoxicology* **2022**, *92*, 131−155.

(7) Yamaguchi, S.; Isaka, R.; Sakahashi, Y.; Tsujino, H.; Haga, Y.; Higashisaka, K.; Tsutsumi, Y. Silver Nanoparticles Suppress Retinoic Acid-Induced Neuronal Differentiation in Human-Derived Neuroblastoma SH-SY5Y Cells. *ACS Appl. Nanomater.* **2022**, *5* (12), 19025−19034.

(8) Skotak, M.; Wang, F.; Chandra, N. An in vitro injury model for SH-SY5Y neuroblastoma cells: effect of strain and strain rate. *J. Neurosci. Methods* **2012**, *205* (1), 159−168.

(9) Cheung, Y.-T.; Lau, W. K.-W.; Yu, M.-S.; Lai, C. S.-W.; Yeung, S.-C.; So, K.-F.; Chang, R. C.-C. Effects of all-trans-retinoic acid on human SH-SY5Y neuroblastoma as in vitro model in neurotoxicity research. *Neurotoxicology* **2009**, *30* (1), 127−135.

(10) Ganguly, U.; Ganguly, A.; Sen, O.; Ganguly, G.; Cappai, R.; Sahoo, A.; Chakrabarti, S. Dopamine cytotoxicity on SH-SY5Y cells: Involvement of α-synuclein and relevance in the neurodegeneration of sporadic Parkinson's disease. *Neurotox. Res.* **2019**, *35* (4), 898−907.

(11) Xicoy, H.; Wieringa, B.; Martens, G. J. The SH-SY5Y cell line in Parkinson's disease research: a systematic review. *Mol. Neurodegener.* **2017**, *12* (1), 10.

(12) Jämsä, A.; Hasslund, K.; Cowburn, R. F.; Bäckström, A.; Vasänge, M. The retinoic acid and brain-derived neurotrophic factor differentiated SH-SY5Y cell line as a model for Alzheimer's disease-like tau phosphorylation. *Biochem. Biophys. Res. Commun.* **2004**, *319* (3), 993−1000.

(13) Berardi, N.; Pizzorusso, T.; Maffei, L. Critical periods during sensory development. *Curr. Opin. Neurobiol.* **2000**, *10* (1), 138−145.

(14) Janesick, A.; Wu, S. C.; Blumberg, B. Retinoic acid signaling and neuronal differentiation. *Cell. Mol. Life Sci.* **2015**, *72* (8), 1559−1576.

(15) Påhlman, S.; Ruusala, A.-I.; Abrahamsson, L.; Mattsson, M. E.; Esscher, T. Retinoic acid-induced differentiation of cultured human neuroblastoma cells: a comparison with phorbolester-induced differentiation. *Cell Differ.* **1984**, *14* (2), 135−144.

(16) Lopes, F. M.; Schröder, R.; da Frota Júnior, M. L. C.; Zanotto-Filho, A.; Müller, C. B.; Pires, A. S.; Meurer, R. T.; Colpo, G. D.; Gelain, D. P.; Kapczinski, F. Comparison between proliferative and neuron-like SH-SY5Y cells as an in vitro model for Parkinson disease studies. *Brain Res.* **2010**, *1337*, 85−94.

(17) López-Carballo, G.; Moreno, L.; Masiá, S.; Pérez, P.; Barettino, D. Activation of the phosphatidylinositol 3-kinase/Akt signaling pathway by retinoic acid is required for neural differentiation of SH-SY5Y human neuroblastoma cells. *J. Biol. Chem.* **2002**, *277* (28), 25297−25304.

(18) Maden, M. Retinoic acid in the development, regeneration and maintenance of the nervous system. *Nat. Rev. Neurosci.* **2007**, *8* (10), 755−765.

(19) Teppola, H.; Sarkanen, J.-R.; Jalonen, T. O.; Linne, M.-L. Morphological Differentiation Towards Neuronal Phenotype of SH-SY5Y Neuroblastoma Cells by Estradiol, Retinoic Acid and Cholesterol. *Neurochem. Res.* **2016**, *41* (4), 731−747.

(20) Filograna, R.; Civiero, L.; Ferrari, V.; Codolo, G.; Greggio, E.; Bubacco, L.; Beltramini, M.; Bisaglia, M. Analysis of the Catecholaminergic Phenotype in Human SH-SY5Y and BE(2)-M17 Neuroblastoma Cell Lines upon Differentiation. *PLoS One* **2015**, *10* (8), e0136769.

(21) Katsetos, C. D.; Herman, M. M.; Mörk, S. J. Class III β-tubulin in human development and cancer. *Cell Motil. Cytoskeleton* **2003**, *55* (2), 77−96.

(22) Dennis, K.; Uittenbogaard, M.; Chiaramello, A.; Moody, S. A. Cloning and characterization of the 5′-flanking region of the rat neuron-specific Class III β-tubulin gene. *Gene* **2002**, *294* (1−2), 269−277.

(23) Katsetos, C. D.; Frankfurter, A.; Christakos, S.; Mancall, E. L.; Vlachos, I. N.; Urich, H. Differential localization of class III β-tubulin isotype and calbindin-D28k defines distinct neuronal types in the developing human cerebellar cortex. *J. Neuropath. Exp. Neurol.* **1993**, *52* (6), 655−666.

(24) McAllister, A. K. Neurotrophins and neuronal differentiation in the central nervous system. *Cell. Mol. Life Sci.* **2001**, *58* (8), 1054−1060.

(25) Truckenmiller, M.; Vawter, M. P.; Cheadle, C.; Coggiano, M.; Donovan, D. M.; Freed, W. J.; Becker, K. G. Gene expression profile in early stage of retinoic acid-induced differentiation of human SH-SY5Y neuroblastoma cells. *Restor. Neurol. Neurosci.* **2001**, *18* (2−3), 67−80.

(26) de Bittencourt Pasquali, M. A.; de Ramos, V. M.; Albanus, R. D.; Kunzler, A.; de Souza, L. H. T.; Dalmolin, R. J. S.; Gelain, D. P.; Ribeiro, L.; Carro, L.; Moreira, J. C. F. Gene expression profile of NF-κB, Nrf2, glycolytic, and p53 pathways during the SH-SY5Y neuronal differentiation mediated by retinoic acid. *Mol. Neurobiol.* **2016**, *53* (1), 423−435.

(27) Korecka, J. A.; van Kesteren, R. E.; Blaas, E.; Spitzer, S. O.; Kamstra, J. H.; Smit, A. B.; Swaab, D. F.; Verhaagen, J.; Bossers, K. Phenotypic characterization of retinoic acid differentiated SH-SY5Y cells by transcriptional profiling. *PloS One* **2013**, *8* (5), e63862.

(28) Goldie, B. J.; Barnett, M. M.; Cairns, M. J. BDNF and the maturation of posttranscriptional regulatory networks in human SH-SY5Y neuroblast differentiation. *Front. Cell. Neurosci.* **2014**, *8*, 325−331.

(29) Barth, M.; Toto Nienguesso, A.; Navarrete Santos, A.; Schmidt, C. Quantitative proteomics and in-cell cross-linking reveal cellular

reorganisation during early neuronal differentiation of SH-SY5Y cells. *Communi. Biol.* **2022**, *5* (1), 551.
(30) Jahn, K.; Wieltsch, C.; Blumer, N.; Mehlich, M.; Pathak, H.; Khan, A. Q.; Hildebrandt, H.; Frieling, H. A cell culture model for investigation of synapse influenceability: epigenetics, expression and function of gene targets important for synapse formation and preservation in SH-SY5Y neuroblastoma cells differentiated by retinoic acid. *J. Neural Transm.* **2017**, *124* (11), 1341−1367.
(31) Paoletti, L.; Elena, C.; Domizi, P.; Banchio, C. Role of phosphatidylcholine during neuronal differentiation. *IUBMB Life* **2011**, *63* (9), 714−720.
(32) Hirabayashi, Y.; Furuya, S. Roles of l-serine and sphingolipid synthesis in brain development and neuronal survival. *Prog. Lipid Res.* **2008**, *47* (3), 188−203.
(33) Mitoma, J.; Furuya, S.; Hirabayashi, Y. A novel metabolic communication between neurons and astrocytes: non-essential amino acid L-serine released from astrocytes is essential for developing hippocampal neurons. *Neurosci. Res.* **1998**, *30* (2), 195−199.
(34) Jacobson, K.; Mouritsen, O. G.; Anderson, R. G. Lipid rafts: at a crossroad between cell biology and physics. *Nat. Cell Biol.* **2007**, *9* (1), 7−14.
(35) Zhang, T.; Gygi, S. P.; Paulo, J. A. Temporal Proteomic Profiling of SH-SY5Y Differentiation with Retinoic Acid Using FAIMS and Real-Time Searching. *J. Proteome Res.* **2021**, *20* (1), 704−714.
(36) Atilla-Gokcumen, G. E.; Castoreno, A. B.; Sasse, S.; Eggert, U. S. Making the cut: the chemical biology of cytokinesis. *ACS Chem. Biol.* **2010**, *5* (1), 79−90.
(37) Atilla-Gokcumen, G.; Bedigian, A.; Sasse, S.; Eggert, U. Inhibition of glycosphingolipid biosynthesis induces cytokinesis failure. *J. Am. Chem. Soc.* **2011**, *133* (26), 10010−10013.
(38) Hsu, F.-F.; Ma, Z.; Wohltmann, M.; Bohrer, A.; Nowatzke, W.; Ramanadham, S.; Turk, J. Electrospray ionization/mass spectrometric analyses of human promonocytic U937 cell glycerolipids and evidence that differentiation is associated with membrane lipid composition changes that facilitate phospholipase A2 activation. *J. Biol. Chem.* **2000**, *275* (22), 16579−16589.
(39) Postle, A. D.; Gonzales, L. W.; Bernhard, W.; Clark, G. T.; Godinez, M. H.; Godinez, R. I.; Ballard, P. L. Lipidomics of cellular and secreted phospholipids from differentiated human fetal type II alveolar epithelial cells. *J. Lipid Res.* **2006**, *47* (6), 1322−1331.
(40) Presgraves, S. P.; Ahmed, T.; Borwege, S.; Joyce, J. N. Terminally differentiated SH-SY5Y cells provide a model system for studying neuroprotective effects of dopamine agonists. *Neurotox. Res.* **2003**, *5* (8), 579−598.
(41) Biedler, J. L.; Helson, L.; Spengler, B. A. Morphology and growth, tumorigenicity, and cytogenetics of human neuroblastoma cells in continuous culture. *Cancer Res.* **1973**, *33* (11), 2643−2652.
(42) Shipley, M. M.; Mangold, C. A.; Szpara, M. L. Differentiation of the SH-SY5Y Human Neuroblastoma Cell Line. *JoVE* **2016**, *108*, e53193.
(43) Numakawa, T.; Suzuki, S.; Kumamaru, E.; Adachi, N.; Richards, M.; Kunugi, H. BDNF function and intracellular signaling in neurons. *Histol. Histopathol.* **2010**, *25* (2), 237−258.
(44) Paik, S.; Somvanshi, R. K.; Kumar, U. Somatostatin-Mediated Changes in Microtubule-Associated Proteins and Retinoic Acid−Induced Neurite Outgrowth in SH-SY5Y Cells. *J. Mol. Neurosci.* **2019**, *68* (1), 120−134.
(45) Murillo, J. R.; Goto-Silva, L.; Sánchez, A.; Nogueira, F. C.; Domont, G. B.; Junqueira, M. Quantitative proteomic analysis identifies proteins and pathways related to neuronal development in differentiated SH-SY5Y neuroblastoma cells. *EuPA Open Proteom.* **2017**, *16*, 1−11.
(46) Simões, R. F.; Ferrão, R.; Silva, M. R.; Pinho, S. L.; Ferreira, L.; Oliveira, P. J.; Cunha-Oliveira, T. Refinement of a differentiation protocol using neuroblastoma SH-SY5Y cells for use in neurotoxicology research. *Food Chem. Toxicol.* **2021**, *149*, 111967.
(47) Millner, A.; Lizardo, D. Y.; Atilla-Gokcumen, G. E. Untargeted Lipidomics Highlight the Depletion of Deoxyceramides during Therapy-Induced Senescence. *Proteomics* **2020**, *20* (10), e2000013.
(48) Fahy, E.; Subramaniam, S.; Murphy, R. C.; Nishijima, M.; Raetz, C. R.; Shimizu, T.; Spener, F.; van Meer, G.; Wakelam, M. J.; Dennis, E. A. Update of the LIPID MAPS comprehensive classification system for lipids1. *J. Lipid Res.* **2009**, *50*, S9−S14.
(49) Li, L.; Li, R.; Zhou, J.; Zuniga, A.; Stanislaus, A. E.; Wu, Y.; Huan, T.; Zheng, J.; Shi, Y.; Wishart, D. S.; et al. MyCompoundID: Using an Evidence-Based Metabolome Library for Metabolite Identification. *Anal. Chem.* **2013**, *85* (6), 3401−3408.
(50) Wishart, D. S.; Tzur, D.; Knox, C.; Eisner, R.; Guo, A. C.; Young, N.; Cheng, D.; Jewell, K.; Arndt, D.; Sawhney, S. HMDB: the human metabolome database. *Nucleic Acids Res.* **2007**, *35*, D521−D526.
(51) Huan, T.; Tang, C.; Li, R.; Shi, Y.; Lin, G.; Li, L. MyCompoundID MS/MS Search: Metabolite Identification Using a Library of Predicted Fragment-Ion-Spectra of 383,830 Possible Human Metabolites. *Anal. Chem.* **2015**, *87* (20), 10619−10626.
(52) Genaro-Mattos, T. C.; Anderson, A.; Allen, L. B.; Korade, Z.; Mirnics, K. Cholesterol Biosynthesis and Uptake in Developing Neurons. *ACS Chem. Neurosci.* **2019**, *10* (8), 3671−3681.
(53) Ferris, H. A.; Perry, R. J.; Moreira, G. V.; Shulman, G. I.; Horton, J. D.; Kahn, C. R. Loss of astrocyte cholesterol synthesis disrupts neuronal function and alters whole-body metabolism. *Proc. Natl. Acad. Sci. U. S. A.* **2017**, *114* (5), 1189−1194.
(54) Roth, K.; Yang, Z.; Agarwal, M.; Liu, W.; Peng, Z.; Long, Z.; Birbeck, J.; Westrick, J.; Liu, W.; Petriello, M. C. Exposure to a mixture of legacy, alternative, and replacement per-and polyfluoroalkyl substances (PFAS) results in sex-dependent modulation of cholesterol metabolism and liver injury. *Environ. Int.* **2021**, *157*, 106843.
(55) Kadowaki, H.; Grant, M. A. Relationship of membrane phospholipid composition, lactosylceramide molecular species, and the specificity of CMP-N-acetylneuraminate: lactosylceramide alpha 2, 3-sialyltransferase to the molecular species composition of GM3 ganglioside. *J. Lipid Res.* **1995**, *36* (6), 1274−1282.
(56) Marcucci, H.; Paoletti, L.; Jackowski, S.; Banchio, C. Phosphatidylcholine biosynthesis during neuronal differentiation and its role in cell fate determination. *J. Biol. Chem.* **2010**, *285* (33), 25382−25393.
(57) Hussain, G.; Wang, J.; Rasul, A.; Anwar, H.; Imran, A.; Qasim, M.; Zafar, S.; Kamran, S. K. S.; Razzaq, A.; Aziz, N. Role of cholesterol and sphingolipids in brain development and neurological diseases. *Lipids Health Dis.* **2019**, *18* (1), 26.
(58) Olsen, A. S. B.; Færgeman, N. J. Sphingolipids: membrane microdomains in brain development, function and neurological diseases. *Open Biol.* **2017**, *7* (5), 170069.
(59) Furuya, S.; Mitoma, J.; Makino, A.; Hirabayashi, Y. Ceramide and its interconvertible metabolite sphingosine function as indispensable lipid factors involved in survival and dendritic differentiation of cerebellar Purkinje cells. *J. Neurochem.* **1998**, *71* (1), 366−377.
(60) Cook, H.; Clarke, J.; Spence, M. Involvement of triacylglycerol in the metabolism of fatty acids by cultured neuroblastoma and glioma cells. *J. Lipid Res.* **1982**, *23* (9), 1292−1300.
(61) Nieweg, K.; Schaller, H.; Pfrieger, F. W. Marked differences in cholesterol synthesis between neurons and glial cells from postnatal rats. *J. Neurochem.* **2009**, *109* (1), 125−134.
(62) Tracey, T. J.; Steyn, F. J.; Wolvetang, E. J.; Ngo, S. T. Neuronal lipid metabolism: multiple pathways driving functional outcomes in health and disease. *Front. Mol. Neurosci.* **2018**, *11*, 10.
(63) Cook, H. W. Metabolism of triacylglycerol in developing rat brain. *Neurochem. Res.* **1981**, *6* (11), 1217−1229.
(64) Coleman, R. A.; Mashek, D. G. Mammalian Triacylglycerol Metabolism: Synthesis, Lipolysis, and Signaling. *Chem. Rev.* **2011**, *111* (10), 6359−6386.
(65) Buccoliero, R.; Bodennec, J.; Futerman, A. H. The role of sphingolipids in neuronal development: lessons from models of sphingolipid storage diseases. *Neurochem. Res.* **2002**, *27*, 565−574.

https://doi.org/10.1021/envhealth.3c00022
Environ. Health 2023, 1, 110−120

(66) van Echten-Deckert, G.; Herget, T. Sphingolipid metabolism in neural cells. *Biochim. Biophys. Acta Biomembr.* **2006**, *1758* (12), 1978−1994.
(67) Harel, R.; Futerman, A. H. Inhibition of sphingolipid synthesis affects axonal outgrowth in cultured hippocampal neurons. *J. Biol. Chem.* **1993**, *268* (19), 14476−14481.
(68) Carrizo, D.; Chevallier, O. P.; Woodside, J. V.; Brennan, S. F.; Cantwell, M. M.; Cuskelly, G.; Elliott, C. T. Untargeted metabolomic analysis of human serum samples associated with exposure levels of Persistent organic pollutants indicate important perturbations in Sphingolipids and Glycerophospholipids levels. *Chemosphere* **2017**, *168*, 731−738.
(69) Li, X.; Li, T.; Wang, Z.; Wei, J.; Liu, J.; Zhang, Y.; Zhao, Z. Distribution of perfluorooctane sulfonate in mice and its effect on liver lipidomic. *Talanta* **2021**, *226*, 122150.

https://doi.org/10.1021/envhealth.3c00022
Environ. Health 2023, 1, 110−120